Science of the Total Environment 725 (2020) 138272

Contents lists available at ScienceDirect

Science of the Total Environment

journal homepage: www.elsevier.com/locate/scitotenv

Diatom evidence for mid-Holocene peatland water-table variations and their possible link to solar forcing

Nannan Li [a,b,c], Mengzhen Li [c], Dorothy Sack [d], Wengang Kang [e], Lina Song [c], Yue Yang [c], Yazhuo Zong [c], Dongmei Jie [a,b,c,f,*]

[a] Institute for Peat and Mire Research, State Environmental Protection Key Laboratory of Wetland Ecology and Vegetation Restoration, Northeast Normal University, Renmin 5268, Changchun 130024, China
[b] Key Laboratory of Geographical Processes and Ecological Security in Changbai Mountains, Ministry of Education, Changchun 130024, China
[c] School of Geographical Sciences, Northeast Normal University, Renmin 5268, Changchun 130024, China
[d] Department of Geography, Ohio University, Athens, OH 45701, USA
[e] Institute of Geosystems and Bioindication, Technische Universität Braunschweig, Langer Kamp 19C, 38106 Braunschweig, Germany
[f] Key Laboratory of Vegetation Ecology, Ministry of Education, Changchun 130024, China

HIGHLIGHTS

- Diatoms were used to investigate peatland hydrological change from the EAM margin.
- Water-table is an important factor driving the variations of peatland diatom assemblages.
- Peatland water-table fluctuations follow EASM intensity change since the mid-Holocene.
- Solar insolation is most likely modulating the water-table variations in peatlands.

GRAPHICAL ABSTRACT

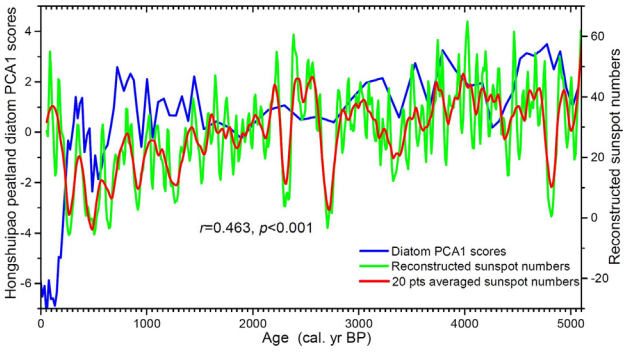

ARTICLE INFO

Article history:
Received 24 November 2019
Received in revised form 15 March 2020
Accepted 26 March 2020
Available online 30 March 2020

Editor: Ouyang Wei

Keywords:
Holocene
East Asian monsoon margin area
Peatland
Solar irradiation
Water-table

ABSTRACT

Peatlands located at the northern edge of the East Asian monsoon (EAM) are well placed to provide a terrestrial record of past climate and hydrological changes for this globally sensitive region. Here we present a middle to late Holocene, diatom-derived water-table records from a peatland in the Greater Hinggan Mountains, northeastern China. An age-depth model was achieved through AMS ^{14}C dating and Bayesian piece-wise linear accumulation modelling. The diatom-based water-table reconstructions show that the peatland water-table rose from 5100 to 3500 cal. yr BP, but fell approximately 3500 cal. yr BP. From about 2800 to 1500 cal. yr BP, the peatland water-table stabilized. After about 1500 cal. yr BP, several rapid hydrological shifts, which correspond with global climate anomalies such as ice-rafted debris (IRD) events, were registered in the reconstructed water-tables. Compared with other paleoclimate records in East Asia, the general trend of peatland water-table fluctuations follows the variations in the East Asian summer monsoon (EASM) intensity. Spectrum analysis of the water-table profile yielded a statistically significant periodicity of 470-year that may be related to the "~500-year" inherent solar irradiation cycles. In addition, positive correlation between the peatland water-table levels and cosmic-isotope-reconstructed sunspot numbers underscores the role of the sun in regulating hydrological processes in the

* Corresponding author at: School of Geographical Sciences, Northeast Normal University, Renmin 5268, Changchun 130024, China.
E-mail address: jiedongmei@nenu.edu.cn (D. Jie).

https://doi.org/10.1016/j.scitotenv.2020.138272

EASM margin area. The data suggest that the regional climate and hydrological variations at the EASM margin were first triggered by changes in solar output, but may have been amplified by interactions with oceanic and atmospheric circulations.

1. Introduction

The East Asian monsoon (EAM) is one of the most important global climate circulation systems (An, 2000; P. Wang et al., 2005; Wang et al., 2017), sustaining more than one third of the world's population (Ding et al., 2010; An et al., 2015). The northern monsoon margin region, also known as the forest-steppe ecotone (Liu et al., 2002), is highly vulnerable to monsoon rainfall and temperature anomalies, since small changes in monsoon temperature or precipitation can trigger great ecological and hydrological shifts in these areas (Liu et al., 2002, 2014; Hao et al., 2016). Climate simulations have indicated that future global warming could induce severe environmental consequences in monsoon margin areas (Zhang et al., 2003; Lioubimtseva and Henebry, 2009), including changes in land cover and land use (Sivakumar, 2007) and in global aeolian dust emissions (Zhang et al., 2003). Given the outlook for future climate change, studies of the monsoon margin area are now more important than ever owing to its sensitive response to global change (Liu et al., 2002, 2014; Hao et al., 2016). A better understanding of the paleoclimate and paleohydrological processes and their potential forcing mechanisms in this region is critical for predicting and assessing their future hydrological and ecological changes (Xiao et al., 2004, 2008; Blaauw and Christen, 2005; Wen et al., 2010, 2017; Fan et al., 2016, 2017).

Increasing availability of Holocene paleoclimate reconstructions that are well dated and of high sampling resolution has greatly improved our knowledge about past climate change and its possible forcing mechanisms at the East Asian monsoon margin (e.g., Xiao et al., 2004, 2008; Wen et al., 2010; Liu et al., 2014; Fan et al., 2016; Hao et al., 2016). Previous studies of lacustrine sediments have underlined the importance of Northern Hemisphere summer insolation variations and high-latitude climate processes (e.g., ice-rafted debris in the North Atlantic) in regulating the regional climate and hydrology at the East Asian monsoon margin (Fan et al., 2016; Wen et al., 2017). However, most recent investigations have been restricted to the middle latitudes and to lacustrine sediments (Wen et al., 2010), whereas the poleward side of the monsoon margin area has been studied only sparsely (Wen et al., 2010; Gao et al., 2018). This imbalance increases the uncertainties and complexities in predicting the ecological impacts of ongoing climate change for the whole monsoon marginal area. Thus, paleoenvironmental records from the higher latitude part of the monsoon margin are needed for an improved understanding of paleoclimate and paleohydrological variations and associated mechanisms, and will aid in assessing the effects of future climate change on these regions.

Peatlands can provide important records of terrestrial paleoenvironmental change and are increasingly acknowledged as excellent natural archives of past environmental variation since accumulation of peat deposits could yield continuous records of climatic change with a high temporal resolution (Chambers and Charman, 2004; Chambers et al., 2012). Employing a variety of proxy data (Blaauw and Christen, 2005), peat-based paleoclimate reconstructions have increased for EAM area in general (e.g., Hong et al., 2000, 2001; Zhou et al., 2010; Li et al., 2017; Liu et al., 2019; Zhang et al., 2019). Diatoms are unicellular, siliceous algae that inhabit a variety of aquatic environments, including peatlands (Gaiser and Rühland, 2010; Hargan et al., 2015a; Chen et al., 2020). They are sensitive to environmental change because of their unique ecological niches and rapid reactions to variations in habitat, especially to water-table, pH, and conductivity changes (Finkelstein et al., 2014; Hargan et al., 2015a, 2015b; Chen et al., 2016; Ma et al., 2018; Gross and Bécares, 2020; Nohe et al., 2020; Rodríguez-Alcalá et al., 2020; Wang et al., 2020). Diatoms have been employed as a proxy for peatland paleoenvironmental change (Rühland et al., 2000; Kokfelt et al., 2009; Gaiser and Rühland, 2010; Fukumoto et al., 2012; Hargan et al., 2015b; Chen et al., 2016; Ma et al., 2018). Moreover, modern diatom assemblage calibrations and statistics allow quantitative inferences concerning past peatland surface moisture and water chemistry characteristics (Gaiser et al., 1998; Rühland et al., 2000; Kokfelt et al., 2009; Gaiser and Rühland, 2010; Chen et al., 2014; Finkelstein et al., 2014; Hargan et al., 2015a, 2015b; Chen et al., 2016; Gross and Bécares, 2020). Some recent diatom-based paleoenvironmental studies have applied multivariate statistical techniques to help reconstruct past peatland environmental variables, such as water-table fluctuations (e.g., Ma et al., 2018; Chen et al., 2020). Those studies demonstrate the important role that diatoms can play in reconstructing peatland paleohydrological variations and dynamics (Hargan et al., 2015a, 2015b; Chen et al., 2016, 2020; Ma et al., 2018).

Because of few records from the northern part of the East Asian monsoon margin and the sensitive response of diatom assemblages to peatland micro-environmental change, this study focuses on diatom analysis of a radiocarbon-dated peat core recovered from the Greater Hinggan Mountains of China. Employing principal component analysis (PCA) and spectral analyses, the present work aims to address the following questions: (1) Are there clear associations between diatom assemblages and peatland environmental variables? (2) What is the main factor that drives the variations in diatom assemblages in a peat core? (3) Do changes in external forcing (or site-specific variables) contribute to peatland paleoenvironment change, and (4) Which types of external forcing, if any, are the major contributors to peatland paleohydrological changes within the East Asian monsoon margin?

2. Materials and methods

2.1. Regional setting and sample collection

The Hongshuipao (HSP) peatland (46°58′55.01″N, 120°50′47.47″E, elevation 778 m) is located in the middle of the Greater Hinggan Mountains (Fig. 1) at the northern margin of the East Asian summer monsoon. The regional climate is influenced by the East Asian monsoon system and the westerlies (Gao et al., 2018). The modern climate pattern of this region displays high seasonal variability. The mean temperature and precipitation for July are 17.1 °C and 115.6 mm; for January they are −24.8 °C and 6.2 mm (China Meteorological Data Service Center, 2019). Summer (June to August) provides >60% of the annual precipitation. The regional vegetation is boreal broadleaf-conifer mixed forest, dominated by plants such as *Larix gmelinii*, *Betula platyphylla*, and *B. dahurica*.

The peatlands formed in the valley of the Tuoxin River, which lies at an elevation of 750 to 760 m and is surrounded by hills with elevations from 900 to 1100 m (Fig. 1). In the summer of 2016, three parallel peat cores (HSP-1, HSP-2, and HSP-3) were collected along an east-west transect in the Hongshuipao peatland using an Eijkelkamp peat sampler. The distance between each core was approximately 10 m. The length for each core was 71 cm, 84 cm, and 74 cm, respectively. The three cores were subsampled at an interval of 1 cm for further analysis.

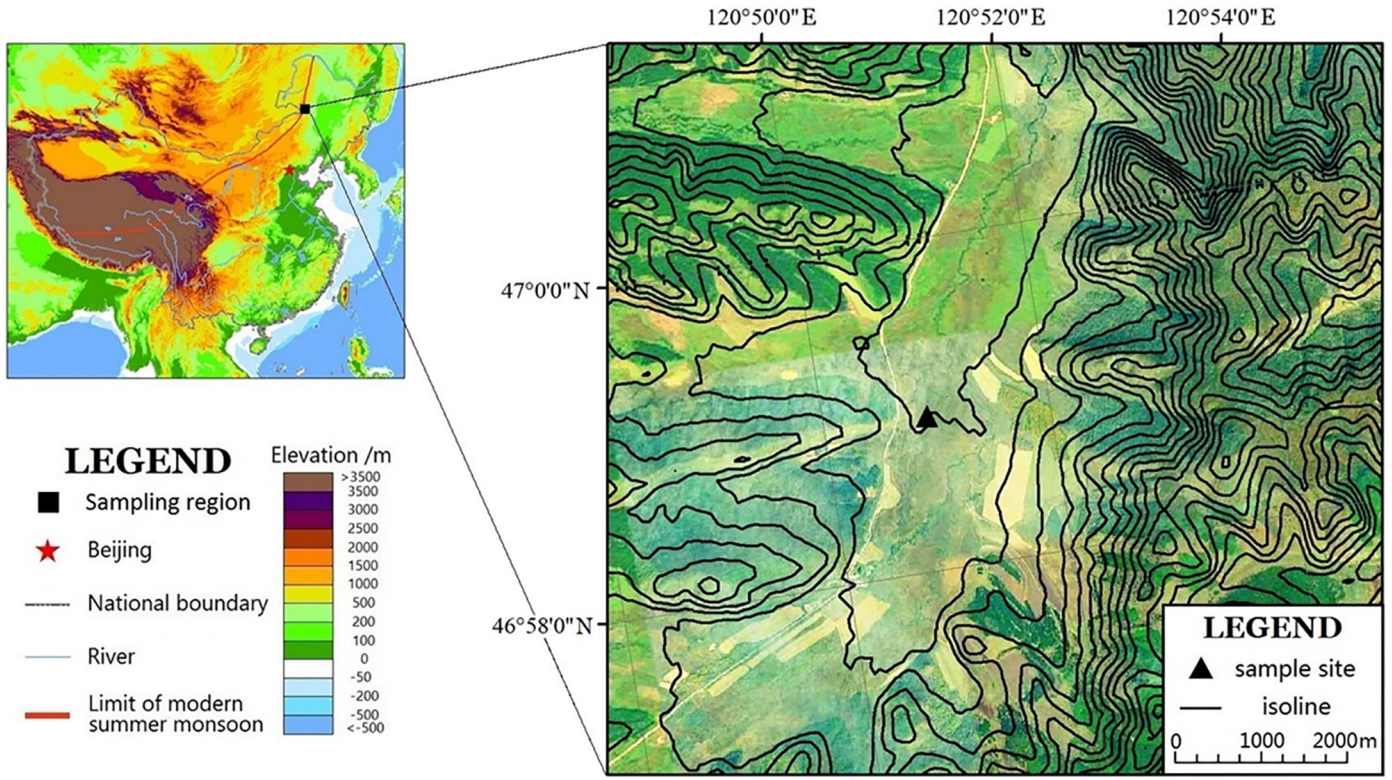

Fig. 1. Location and geographical settings of the Hongshuipao peatland in northeastern China.

2.2. Radiocarbon dating pretreatment and chronological modelling

To establish the age-depth model for each profile, nine samples were collected from the three parallel peat cores for radiocarbon dating. Bulk organic matter was used due to the lack of sufficient terrestrial macrofossils in the sediments. Samples were treated with 1 M HCl (12 h), washed free from acid with Milli-Q water, then dried (65 °C) and homogenized (Piotrowska et al., 2011). The organic carbon in a pretreated sample was converted into CO_2 by combustion with CuO in a sealed quartz tube. After purification, the gas was reduced to graphite by Fe/Zn reduction at Northeast Normal University (Xu et al., 2007). The graphite was then analyzed for ^{14}C activity with Accelerator Mass Spectrometry (AMS) at Guangzhou Institute of Geochemistry, Chinese Academy of Sciences (GIGCAS) (Zhu et al., 2015). In addition, two bulk peat samples were pre-treated and analyzed at the Institute of Accelerator Analysis Ltd., Japan.

All the conventional ^{14}C ages (yr BP) were calibrated into calendar years before present (cal. yr BP) from the IntCal13 calibration curve (Reimer et al., 2013) using the CALIB Rev. 7.04 program and expressed with 2σ ranges (Stuiver and Reimer, 1993). Sampling position, radiocarbon ages, and calibration results are summarized in Table 1. The chronologies were established with Bacon v2.2 in R (Blaauw and Christen, 2011).

2.3. Laboratory analyses

Humification measurements were carried out on the three peat cores. However, because the top 13 cm of sections HSP-1 and HSP-2 were mainly composed of modern plant roots for which it is difficult to measure the humification degree properly, that interval from those two cores were not analyzed for humification. Peat humification was determined using a modified version of the method of Chambers et al. (2011). For each analysis, a 0.1000 g dry and homogenized peat sample was weighed accurately into a 100 mL beaker. Then, 80 mL of 8% NaOH solution was added to the sample. The solution was heated gently for 1 h. After cooling to room temperature, the samples and solutions were separated using a filter and transferred into a 100 mL flask. The amount of humification was then determined from the absorbance of each sample solution at a wavelength of 540 nm (expressed in percentage of absorbance). The measurements were performed with an SP-722 visible spectrophotometer. Analytical precision for the absorbance measurements was 0.1%.

Because core HSP-2 is the longest core of the three peat sections, diatom analyses were conducted on samples collected at 1 cm interval from that core. The diatom samples were pretreated with 10% hydrochloric acid (HCl) and 30% hydrogen peroxide (H_2O_2) until the reaction stopped to remove carbonates and organic matters. The residual was washed in distilled water until nearly neutral (Serieyssol et al., 2010–2011). Diatoms were extracted through heavy liquid ($ZnBr_2$) flotation at a density of 2.30 g/cm^3 (Serieyssol et al., 2010–2011). After washing, each sample was rinsed in distilled water and ethanol and placed on slides in Canada balsam with a refractive index of 1.5216–1.5240 for identification and counting. Diatom identification and counting were carried out using an Olympus BX53 optical light microscope with reference to Krammer and Lange-Bertalot (1986–1991), Hargan et al. (2015a, 2015b), and Chen et al. (2016). A minimum of 260 valves were counted per sample, with the exception of one sample that had a count of 207 valves.

2.4. Statistical and spectral analyses

Diatom data for each sample were expressed as relative abundance (in %) and presented in biostratigraphic profiles using TILIA (Grimm, 1992). From the diatom data, biostratigraphic zones were established by cluster analysis using constrained incremental sum of squares (CONISS) (Grimm, 1987).

Principal component analyses (PCA) were performed to reveal the main factors associated with the variation of diatom assemblages. Prior to PCA, Pearson correlations between different diatom taxa were conducted using the "corrplot" package in R (Wei and Simko, 2017). PCA was performed using the *prcomp()* function in R, and the graphs of eigenvalues and variables were plotted using the R package "factoextra" (Kassambara and Mundt, 2019). All of these statistical analyses were performed in R 3.5.0 (R Core Team, 2017) with RStudio v1.1.463 (RStudio Team, 2016).

Spectral analyses were performed using REDFIT 3.8e (Schulz and Mudelsee, 2002) to extract the periodicities from the unevenly spaced peatland water-tables. The program involves the Lomb-Scargle Fourier transform to overcome unequal time intervals. A first-order autoregressive (AR1) parameter was generated from the dataset and presented in the frequency domain to test whether spectral peaks are significant against the red-noise background generated from a first-order autoregressive process (null hypothesis).

3. Results

3.1. Chronology

Four radiocarbon dates were obtained from peat core HSP-2 (Table 1). The radiocarbon dates for HSP-2 are older than those obtained from the other two cores, indicating possible contamination from the older carbon (Table 1). Contamination with older carbon is further

Table 1
AMS radiocarbon dates and calibrations of samples from the Hongshuipao peatland.

Core no.	Depth (cm)	Lab. code[a]	Material	Pretreatment	AMS ^{14}C yr BP	Uncertainty	2σ-range calibrations with probability	Median age, cal. yr BP
HSP-1	53–54	IAAA-171136[a]	Bulk organic matter	HCl	1030	20	924–966 cal. BP (100%)	945
HSP-1	69–70	NENUR10214	Bulk organic matter	HCl	1670	25	1528–1620 cal. BP (97.84%); 1676–1686 cal. BP (2.16%)	1573
HSP-2	24–25	NENUR10217	Bulk organic matter	HCl	2475	30	2380–2393 cal. BP (1.31%); 2409–2410 cal. BP (0.18%); 2427–2720 cal. BP (98.51%)	2582
HSP-2	40–41	NENUR10218	Bulk organic matter	HCl	4245	40	4629–4636 cal. BP (0.60%); 4642–4679 cal. BP (7.93%); 4688–4762 cal. BP (30.37%); 4798–4871 cal. BP (61.10%)	4826
HSP-2	64–65	NENUR10220	Bulk organic matter	HCl	4230	35	4630–4632 cal. BP (0.27%); 4643–4678 cal. BP (9.76%); 4690–4762 cal. BP (38.81%); 4800–4860 cal. BP (51.16%)	4789
HSP-2	82–83	IAAA-171137[a]	Bulk organic matter	HCl	4410	30	4866–5054 cal. BP (95.04%); 5189–5214 cal. BP (4.08%); 5226–5231 cal. BP (0.33%); 5249–5257 cal. BP (0.55%)	4981
HSP-3	13–14	NENUR10222	Bulk organic matter	HCl	355	20	318–395 cal. BP (50.82%); 424–491 cal. BP (49.18%)	403
HSP-3	41–42	NENUR10224	Bulk organic matter	HCl	2685	35	2750-2851 cal. BP (100%)	2789
HSP-3	64–65	NENUR10225	Bulk organic matter	HCl	3650	40	3866-4088 cal. BP (100%)	3971

[a] Samples were analyzed at the Institute of Accelerator Analysis Ltd., IAA, Japan.

supported by the original dating results showing two identical ages (4245 ± 40 ^{14}C BP and 4230 ± 35 ^{14}C BP) at depth 40–41 cm and 64–65 cm, respectively, in core HSP-2 (Table 1).

Fig. S1 shows that the three humification curves display very similar trends, although small differences do exist. The close similarity among the three humification profiles suggests that they are correlative (Fig. S2). Comparing the humification profiles for the three cores (Figs. S1 and S2) likewise supports the notion that the HSP-2 is contaminated with older carbon. Therefore, the three older radiocarbon dates from HSP-2 were rejected as contaminated, and those provided by the other cores were accepted. From these data, a chronology for the peatland was reconstructed. Table S1 presents all of the ages and their equivalent depths at each core. The chronological model indicates that core HSP-2 recorded the paleoclimate and paleoecological history of Hongshuipao peatland since ca. 5100 cal. yr BP (Fig. 2).

3.2. Diatom assemblages

From peat core HSP-2, 94 species of diatoms were identified from the 82 sediment samples (Krammer and Lange-Bertalot, 1986–1991; Lange-Bertalot et al., 2011; Hargan et al., 2015a; Chen et al., 2016). Fig. 3 shows diatom abundance plotted against depth. Most of these species commonly occurred in freshwater (lake, stream) and peat environments (e.g., *Eunotia* and *Pinnularia*) (Krammer and Lange-Bertalot, 1986–1991; Lange-Bertalot et al., 2011; Hargan et al., 2015a). The diatom assemblages underwent notable shifts throughout the 5100-year sequence, and CONISS identified four first-order diatom stratigraphic zones in HSP-2 (Fig. 3). Three additional second-order subzones (II_a, II_b, and II_c) were identified in Zone II.

Zone I (74 to 84 cm; 5100 to 4500 cal. yr BP) is characterized by the dominance of the diatoms *E. implicata*, *M. circulare*, and *M. criculare* var. *constrictum* (Fig. 3). This suggests that freshwater was flowing in the peatland during that interval (Krammer and Lange-Bertalot, 1986–1991).

Zone II_a (66 to 74 cm; 4500 to 3700 cal. yr BP) is marked by increasing abundances of *Pinnularia* spp. and *H. amphioxys*, and a decrease in *E. implicata* and *M. circulare*. Because *H. amphioxys* and *Pinnularia* spp. are more tolerant than the latter two species to dry and slightly alkaline habitats (Hargan et al., 2015a), it is reasonable to deduce that there is a lowering of the peatland water-table and an increase in salt and/or alkaline content caused by a climate shift. Zone II_b (40 to 66 cm; 3700 to 950 cal. yr BP) is dominated by *Pinnularia* spp. and *H. amphioxys*, with an increasing abundance of *N. elginensis* and decreasing abundance of *F. ulna*. Zone II_c (30 to 40 cm; 950 to 600 cal. yr BP) is characterized by growth in *F. ulna*, *E. implicata*, and *C. meneghiniana* abundances, indicating a rise in the water-table and greater availability of freshwater (Krammer and Lange-Bertalot, 1986–1991; Lange-Bertalot et al., 2011; Hargan et al., 2015a).

Zone III (14 to 30 cm; 600 to 250 cal. yr BP) is dominated by *A. lanceolata* and *H. amphioxys*. The *H. amphioxys* abundance decreases whereas the *M. circulare* and *D. mesodon* increases in taxa abundance compared with Zone II_b, suggesting a habitat environment undergoing a shift from a lower to a higher water-table stage (Krammer and Lange-Bertalot, 1986–1991; Lange-Bertalot et al., 2011).

Pinnularia spp. and *Navicula* species dominate Zone IV (0 to 14 cm; 250 cal. yr BP to present). Diatoms that favor freshwater (e.g., stream and spring) habitats, such as *M. circulare*, *A. lanceolata*, *F. ulna*, and *D. mesodon*, disappear, implying a falling water-table and a possible transformation from a eutrophic fen to an oligotrophic bog (Krammer and Lange-Bertalot, 1986–1991; Lange-Bertalot et al., 2011). In addition, because the *Navicula* and *Pinnularia* taxa have relatively high optima with respect to alkalinity, the peatland pH value and/or conductivity likely increased (Hargan et al., 2015a). Thus, compared with lower zones, the higher abundance of peatland diatom taxa in Zone IV suggests a lower water-table condition accompanied by an increase in alkalinity possibly due to a drier climate for a reduction in available water in the peatland.

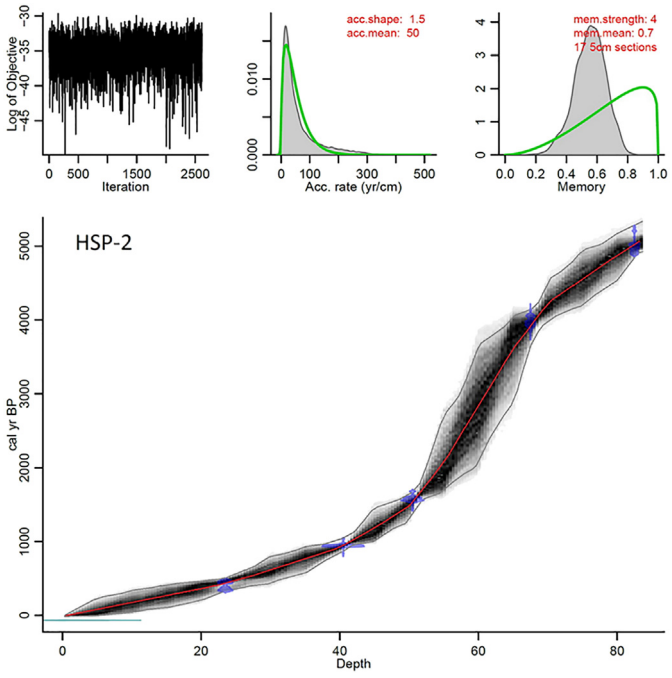

Fig. 2. 'Bacon' age-depth models for HSP-2 peat core. The best estimates for calibrated age are shown in red and the upper and lower estimates are shown in gray.

3.3. Principal component analysis results

The main diatom taxa in core HSP-2 indicate a freshwater, bog-like environment (Lange-Bertalot et al., 2011; Hargan et al., 2015a, 2015b). Although diatoms are abundant in the core, only a few taxa can be used as indicators for micro-habitat change since most diatom types occupy the same or similar habitats (Lange-Bertalot et al., 2011; Hargan et al., 2015a, 2015b; Chen et al., 2016). Pearson correlation analyses show that many diatom species are correlated with each other (Fig. 4), indicating that PCA should be useful for identifying dominant factors that are associated with variations of diatom assemblages.

PCA extracted 6 principal components that together explain 71.04% of the total variance in the input diatom assemblages. Component 1 (axis 1) explains 32.35% of the diatom variations while component (axis) 2 explains 11.05% of the diatom variations (Fig. 5.a). In the species *vs*. PCA plot (Fig. 5.b), diatoms such as *M. circulare*, *M. criculare* var. *constrictum*, *E. implicata*, and *F. ulna* that prefer freshwater (e.g., streams, springs) have the highest positive loadings on axis 1 (Lange-Bertalot et al., 2011; Hargan et al., 2015a; Chen et al., 2016). Epiphytic species that are more tolerant to alkaliphilous and dry habitats (*Pinnularia* spp., *Navicula*, *N. hantzschiana,* and *C. subaequalis* taxa) have high negative loadings on axis 1 (Lange-Bertalot et al., 2011; Hargan et al., 2015a; Chen et al., 2016). *N. elginensis*, *G. acuminatum*, and *F. capucina*, which are usually abundant in eutrophic conditions, have positive loadings along axis 2, whereas *A. lanceolata* has negative loadings along that axis (van Dam et al., 1994; Kelly, 1998; Rott et al., 1998), implying that nutrient conditions of the peatland are regulating the diatom distribution along axis 2. Considering the habitats of the different diatom species, the positive loadings on axis 1 suggest a higher water-table, while the negative ones represent a lower water-table condition. Because the main focus of this study is reconstructing the paleohydrological processes in the Hongshuipao peatland, only principal factor scores of axis 1 were used for peatland water-table reconstructions and related analyses in the following sections.

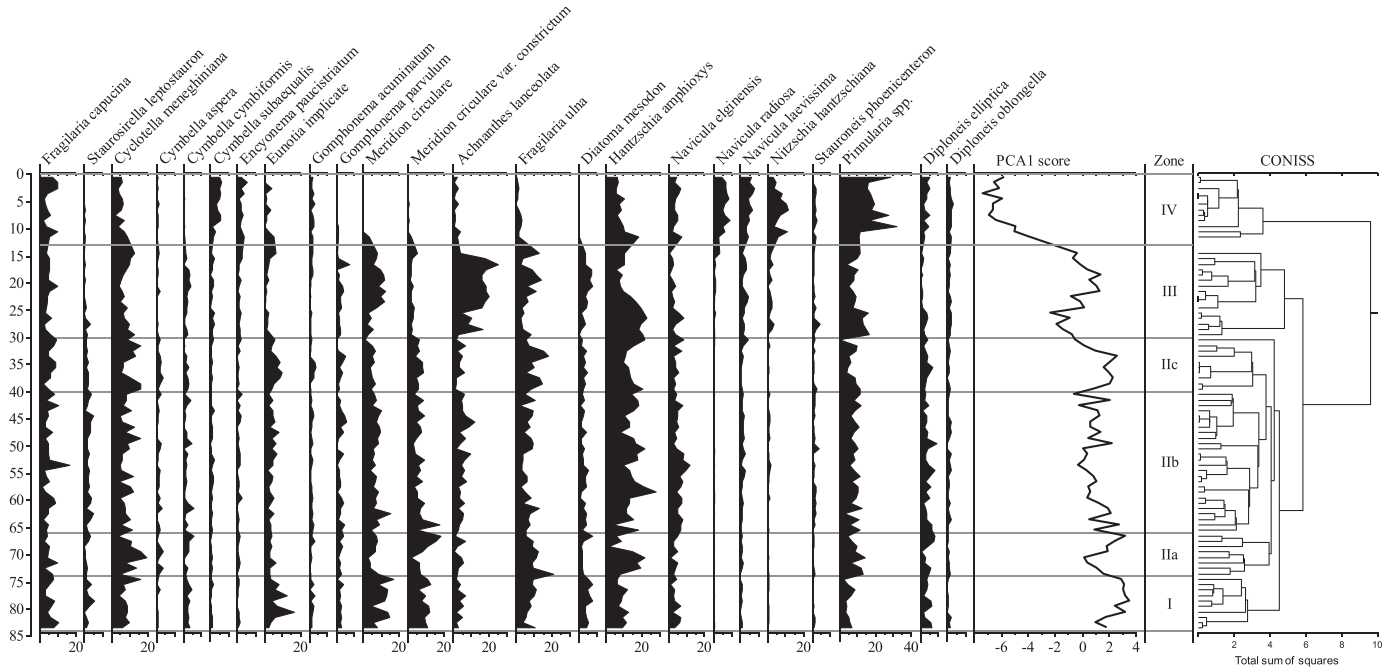

Fig. 3. Diatom stratigraphy diagram showing species abundance (in %) of the peat core HSP-2.

4. Discussion

4.1. Peatland water-table variations since the mid-Holocene

The water-table level in a peatland represents a balance among precipitation, evapotranspiration, surface flows, and groundwater flows (Ingram, 1983; Charman, 2007; Grundling et al., 2015). Among these, precipitation and evapotranspiration are the two dominant factors and are directly or indirectly related to regional climate variables (Charman, 2007; Grundling et al., 2015). The diatom-based water-table reconstructions in the Hongshuipao peatland for the past 5100 cal. yr BP is characterized by a water-table peak between 5100 and 3500 cal. yr BP, stable conditions from 2800 to 1500 cal. yr BP, and several dry-wet fluctuations after 1500 cal. yr BP (Fig. 6). Comparing the principal factor scores (water-table reconstructions) with other regional paleoclimate reconstructions (Fig. 6) shows that the general trend of peatland water-table variations matches well with changes in East Asian summer monsoon (EASM) intensity. This suggests that peatland hydrological variations are primarily influenced by regional climate-related controls rather than site-specific processes. During the period of increased rainfall, when precipitation exceeded evapotranspiration, peatland water-tables rose (Charman, 2007), providing a habitat for diatoms that prefer higher water-tables and even fresh water species. A rainfall deficit would have caused a lowering of peatland water-tables, resulting in a succession of diatom assemblages (Charman, 2007).

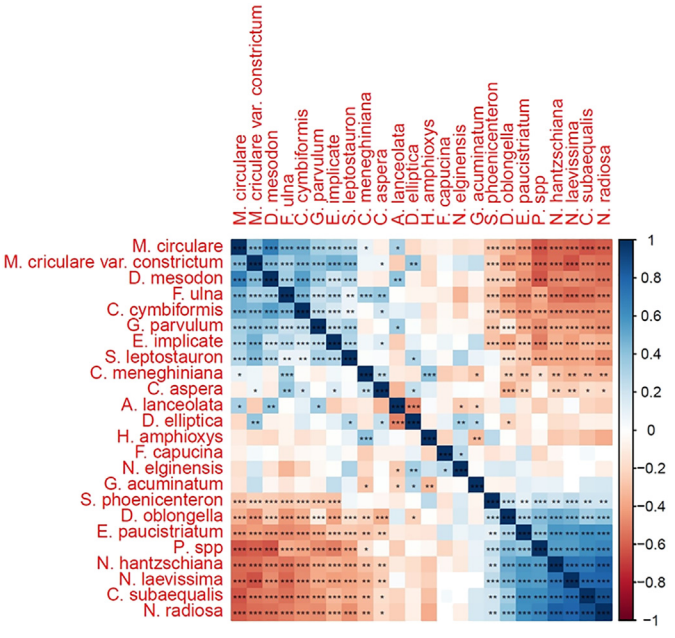

Fig. 4. Correlation matrix, made using the R package "corrplot", between the abundance of main diatom taxa. The legend on the right side of the diagram shows the Pearson correlation coefficients with their corresponding colors. Positive correlations are displayed in blue and negative correlations in red. *, ** and *** denote the statistically significant at $\alpha = 0.05$, $\alpha = 0.01$ and $\alpha = 0.001$, respectively.

The peak in the water-table level between 5100 and 3500 cal. yr BP is likely linked to the Holocene Optimum, evidence for which has been widely reported from the East Asian monsoon area (e.g., Cosford et al., 2009; Wu et al., 2011; Wu et al., 2019). Using *Pinus* and *Quercus* pollen as proxies, Wu et al. (2019) reported a gradually decreased East Asian winter monsoon intensity since ca. 6000 cal. yr BP in the Greater Hinggan Mountains. A mid-Holocene East Asian summer monsoon (EASM) maximum has been registered in stalagmite $\delta^{18}O$ profiles in northern and northeastern China, as evidenced by a negative shift in stalagmite $\delta^{18}O$ values in Lianhua and Nuanhe caves (Cosford et al., 2009; Wu et al., 2011). Geochemical analyses of Lake Dali sediments also show a period of low evaporation and/or humid periods from 4750 to 3200 cal. yr BP, as indicated by smaller Mg/Ca ratios (Fan et al., 2016). Expansion and dominance of broadleaf trees from 5100 to 3800 cal. yr BP has also been identified from a pollen diagram of the Hani peatland (Cui et al., 2006). The high water-table stage indicated here in the Hongshuipao peatland is likely related to an increase in regional precipitation, which is associated with intensified EASM during the mid-Holocene.

After a stage of relatively stable water-table level (2800 to 1500 cal. yr BP) in the Hongshuipao peatland, several rapid water-table shifts occurred (Fig. 6). At the time of the Medieval Warm Period

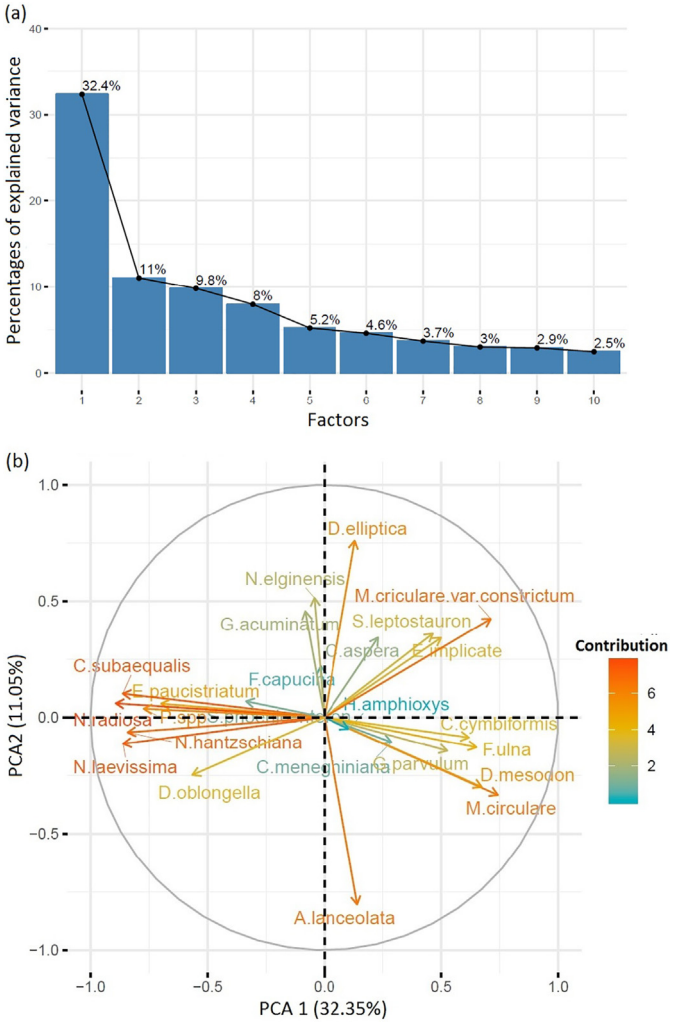

Fig. 5. Principal component analysis (PCA) of diatom variables. (a) Scree plot of principal factors for the diatom assemblages. (b) The principal factor plot showing diatom taxa (variables) and their factor loadings. Contribution is the gradient of quality to highlight the most important variables in explaining the variations retained by the principal components.

(MWP) from 1500 yr to 700 yr (Lamb, 1965; Zhu, 1973), the peatland experienced a high water-table stage that lasted for 800 years. In monsoonal China, this wetter period is also evidenced by a negative shift in stalagmite $\delta^{18}O$ values in Nuanhe Cave (Wu et al., 2011) and increased pollen concentration in a peat core at the Maili peatland from 1000 to 700 cal. yr BP (950 CE–1270 CE), with some pollen taxa reaching their greatest abundance (Ren, 1998). A widespread wet shift from 1500 yr to 700 cal. yr BP has previously been identified in peat α-cellulose $\delta^{18}O$ and $\delta^{13}C$ profiles of the Jinchuan peatland (Hong et al., 2000, 2001). A dramatically lower water-table event occurred in the Hongshuipao peatland from 700 to 400 cal. yr BP, which may correspond to the Little Ice Age (LIA) anomaly. During the same period, in the North Atlantic, the amount of hematite-stained grains increased in marine sediments (Bond et al., 1997, 2001). In East Asia, evidenced by a series of proxies, the LIA-like event has been characterized as a time of decreasing temperature and decreasing precipitation (e.g., Yang et al., 2002; Wang et al., 2007; T. Zhou et al., 2011; X. Zhou et al., 2011). The Hongshuipao peatland water-table rose again from 400 to 250 yr BP. After 250 yr BP, the peatland water-table fell to its lowest level in the profile, which may have resulted from a natural drought event or from human activities. Because of the growing human influence in the last 250 years, identifying the natural climate change signal for that recent interval could be difficult (Guo et al., 2018).

Consistent with other paleoclimate reconstructions in the monsoon region, the general trend of water-table oscillations reconstructed from the Hongshuipao peatland follows the Northern Hemisphere insolation variations (Berger and Loutre, 1991) since the mid-Holocene (Fig. 6). Interestingly, the reconstructed water-tables show close similarity with the stacked ice-rafted debris (IRD) curve in the North Atlantic (Bond et al., 2001). A number of drought shifts at 4500–4200, 3400–3200, 2800–2600, and 700–400 cal. yr BP, were registered in the Hongshuipao peatland water-table profiles (Fig. 6). Those drought events correspond well to some recognized global climate anomalies, e.g., IRD0, IRD2, and IRD3 events in the North Atlantic (Bond et al., 1997, 2001) and the "4.2 ka" aridification event in East Asia (Xiao et al., 2018; Scuderi et al., 2019), suggesting climate teleconnections between the northern part of Asian monsoon margin and global climate and oceanic circulation.

4.2. Periodic oscillation of peatland water-tables and its link to solar forcing

A large number of periodicities have been previously inferred from peat and lacustrine records in monsoonal China (e.g., Hong et al., 2000; Xu et al., 2014; Stebich et al., 2015; Liu et al., 2019; Wu et al., 2019). However, the robustness of many of these periodicities has been questioned as they are highly dependent on the individual age–depth models and may be affected by the data-sampling resolution (Swindles et al., 2007). Redfit analysis performed on the principal factor scores (axis 1) revealed a statistically significant periodicity of 470-year (Fig. 7). The 470-year period is comparable to the ca. 500-year cycle previously reported in the East Asian monsoon area using lake sediments and peat records (e.g., Hong et al., 2000; Xu et al., 2014; Stebich et al., 2015; Wu et al., 2019). For example, from the Jinchuan peatland, a 480-year cycle has been identified in a paleoclimate sequence derived from peat cellulose $\delta^{18}O$ (Hong et al., 2000). This is also similar to the 550- to 600-year cycle derived from quantitative pollen-based paleoclimate reconstructions from Lake Sihailongwan (Stebich et al., 2015) and the ~500-year cycle registered in the pollen records from Lake Xiaolongwan (Xu et al., 2014). Considering that cycles of 512- and 550-year were identified in high-resolution tree ring $\Delta^{14}C$ records (Stuiver and Braziunas, 1993; Stuiver et al., 1995), the approximate 500-year cycle might reflect the inherent solar irradiation oscillations at centennial scales. Therefore, the detection of an approximate 500-year cycle in the Hongshuipao peatland water-table profiles may suggest a possible link between solar output and paleohydrological variations in the East Asian monsoon margin area. Moreover, the consistency between the 470-year cycle determined in this study and other investigations demonstrates that the ~500-year periodicity is persistent in nature, although there may be a certain degree of harmonic reproduction artefacts (Swindles et al., 2007).

Increasing evidence suggests that there is a persistent solar forcing impact on Holocene paleoclimate change in East Asia (e.g., Y. Wang et al., 2005; Liu et al., 2012; Steinhilber et al., 2012; Wu et al., 2019). Visual comparison with the cosmic-isotope-based sunspot number reconstructions suggests that the major wet (dry) phases in the Hongshuipao peatland appear to be associated with increased (decreased) sunspot numbers (Fig. 8). Complexity, however, exists in the timing and amplitude of the paleohydrological responses to the sunspot number fluctuations (Fig. 8). For instance, one interval of lower water-table in the study area (4400–4200 cal. yr BP) that should have approximately coincided with decreased solar activity occurred at a time of greater sunspot numbers (Fig. 8). Uncertainties in the chronological modelling of the peat core is probably the main reasons for this discrepancy. Generally, however, on the basis of the current chronology, the inferred water-table shifts matched well with solar activity, if the age uncertainties of the chronological model are taken into consideration (Figs. 2 and 8).

Pearson correlation confirms the associations between solar forcing and water-table variations in the peatland, except for the period of the last 250 years. The principal factor scores (axis 1) display a positive correlation with cosmic-isotope-based sunspot number reconstructions

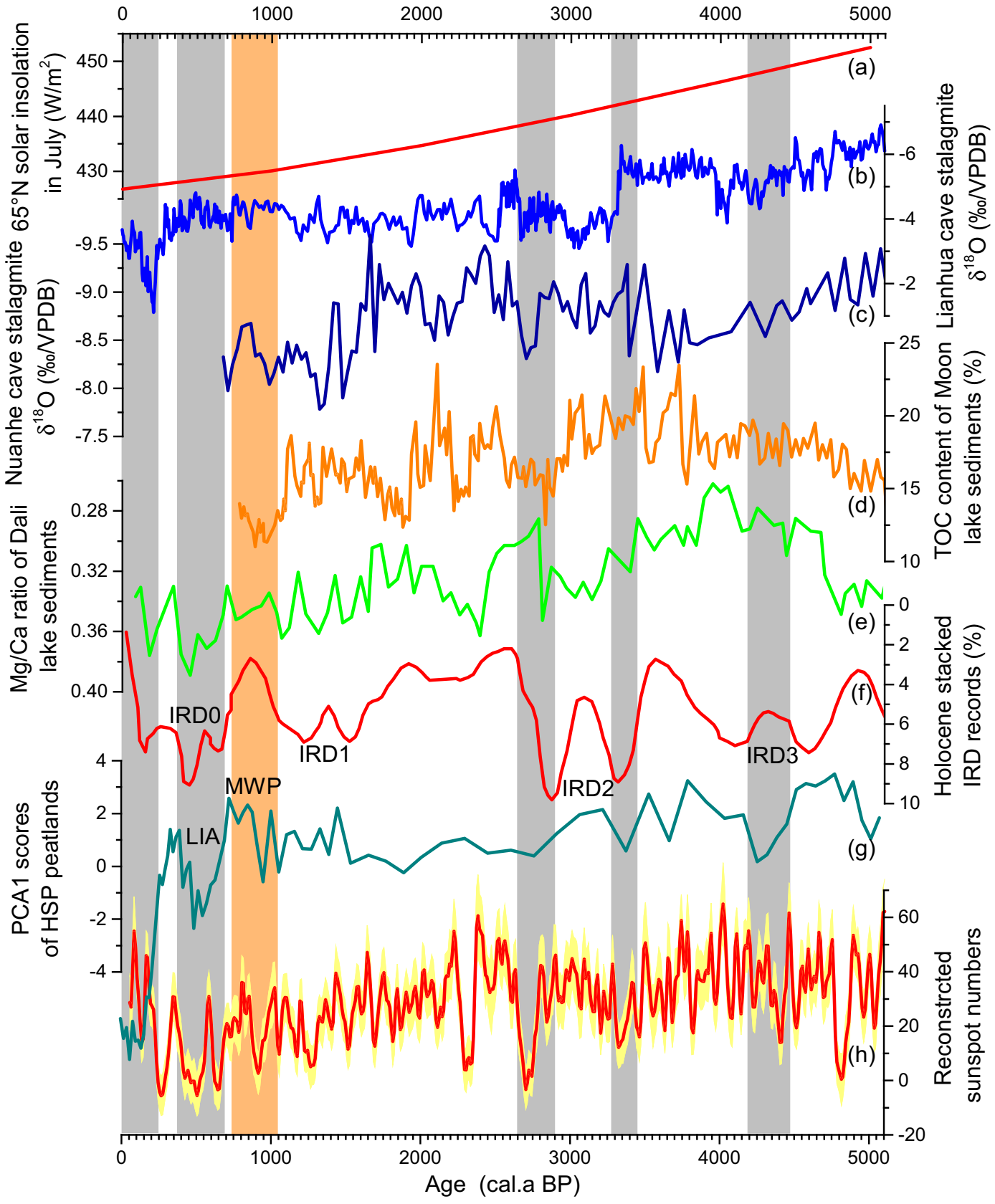

Fig. 6. Comparisons of the Hongshuipao peatland water-table reconstructions with regional and global paleoclimate and solar sequences. (a) North Hemisphere 65° solar irradiation (Berger and Loutre, 1991); (b) stalagmite $\delta^{18}O$ record from Lianhua cave, northern China (Cosford et al., 2009); (c) stalagmite $\delta^{18}O$ record from Nuanhe cave, northeastern China (Wu et al., 2011); (d) TOC content in Lake moon sediments (Liu et al., 2010); (e) Mg/Ca ratio of Lake Dali sediments (Fan et al., 2016); (f) stacked IRD events in North Atlantic (Bond et al., 2001); (g) Hongshuipao peatland water-table reconstructions (this study); (h) cosmic-isotope-based sunspot number reconstructions (Solanki et al., 2004).

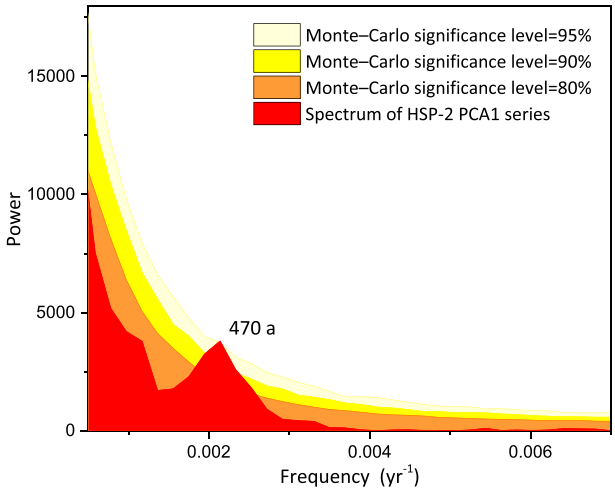

Fig. 7. Spectral analysis of Hongshuipao water-table sequence (diatom based principal factor scores of axis 1). Upper light yellow, yellow and orange areas denote 95%, 90% and 80% confidence of periodicity by Monte-Carlo Test relative to an AR1 background, respectively; power spectra calculated using the REDFIG 3.8e (Schulz and Mudelsee, 2002).

(Solanki et al., 2004) at a statistically significant level ($r = 0.463$, $p < 0.001$, Fig. 8), suggesting solar-paced paleoclimate and paleohydrological changes in the monsoon margin area. However, in the most recent interval (250 cal. yr BP to present), human activities (Guo et al., 2018) may have overshadowed the natural climate change signals, causing obvious discrepancies between peatland water-tables and reconstructed sunspot numbers.

4.3. Possible interpretations for peatland hydrological responses to solar forcing

Globally, the monsoon system is modulated by land *vs.* ocean contrast, sea surface temperatures, and inter-hemispheric heat gradients (Chao and Chen, 2001; P. Wang et al., 2005). Because of the heat capacity difference between the ocean and the continent, the EASM intensity is controlled by the related ocean-land air pressure gradient, which can be influenced by variations in solar irradiation (Chao and Chen, 2001; P. Wang et al., 2005). The present study indicates that water-tables in the Hongshuipao peatland are sensitive to variations in cosmic-isotope reconstructed solar activities. The cosmic rays (solar irradiations) likely affect peatland hydrologic patterns through their influence on regional climates since solar activity is correlated with Earth's surface processes, including temperature and precipitation patterns (Marsh and Svensmark, 2003; Emile-Geay et al., 2007). These, in turn, determine the amount of effective moisture in the peatland.

During periods of increased solar irradiation, a steep ocean/continent air pressure gradient and the northward movement of the ITCZ (P. Wang et al., 2005; Wang et al., 2017; X. Zhou et al., 2011) enhance the intensity of the East Asian summer monsoon (Chao and Chen, 2001; Wang et al., 2017). The strengthened EASM brings maritime air masses (wet and warm) into eastern and northern China, resulting in increased precipitation (X. Zhou et al., 2011) and a rising water-table phase in the Hongshuipao peatland. When solar insolation decreases, the air pressure difference between the Asian continent and the Pacific Ocean is getting smaller, and a weaker EASM brings less moisture to the study area (X. Zhou et al., 2011). Under these conditions, the peatlands at the northern margin of the EAM will experience a water-table lowering.

Although solar irradiation could trigger regional climate change, its direct influence on global climate is quite small (Berger and Loutre, 1991; Haigh, 1996; Shindell et al., 1999, 2001; Emile-Geay et al., 2007). Amplifiers associated with variations in solar irradiation could induce greater regional climate variations that observed in proxy-

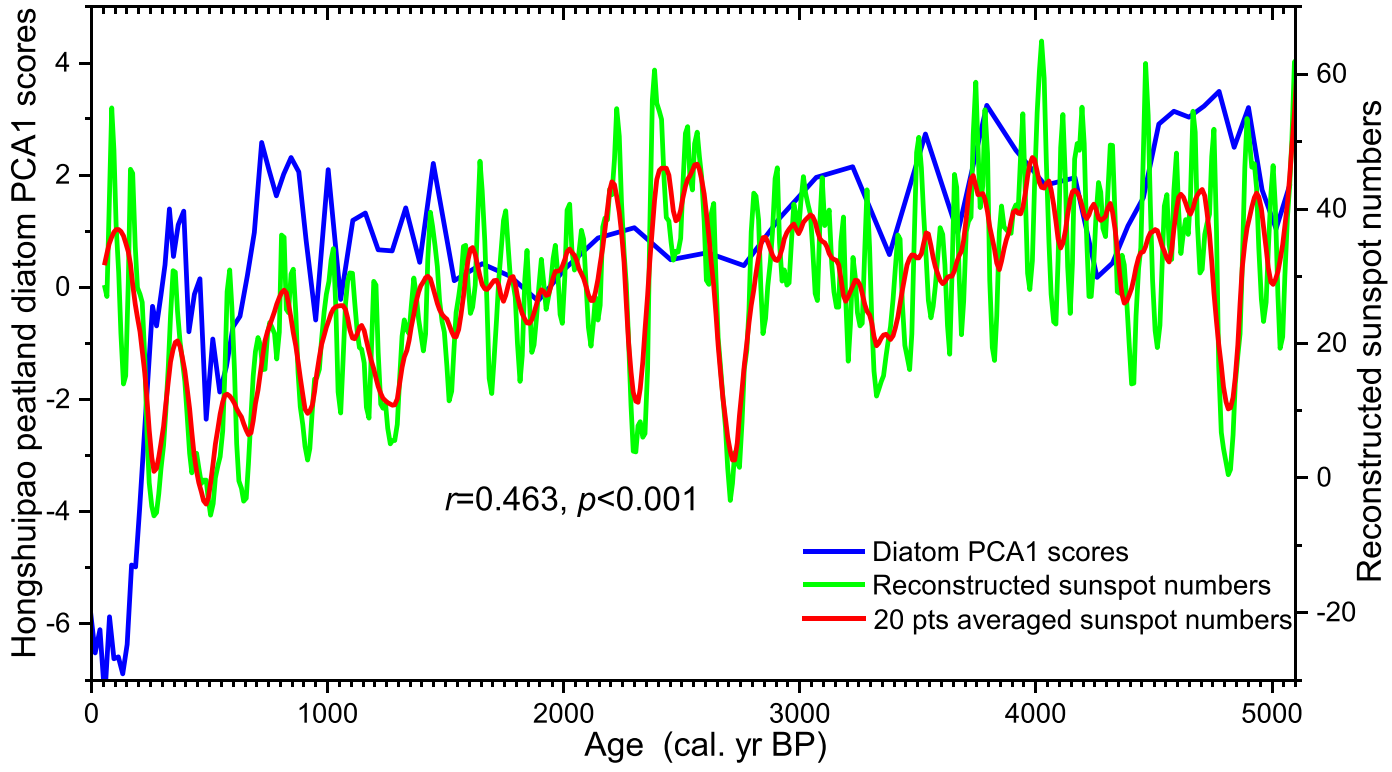

Fig. 8. Co-variation and correlation between the Hongshuipao peatland water-table level variations and the reconstructed sunspot number (Solanki et al., 2004).

based reconstructions (e.g., Shindell et al., 1999, 2001; Emile-Geay et al., 2007; Xu et al., 2014; Liu et al., 2019). In addition to solar forcing, fluctuations in the reconstructed water-table of the Hongshuipao peatland appear to be approximately synchronous with the stacked ice-rafted debris (IRD) events that have been identified in the North Atlantic (Fig. 7). One possible explanation is that reduced solar irradiance may have first increased the polar ice volume, which reduced the North Atlantic deep water (NADW) circulations (Shindell et al., 1999, 2001; Bond et al., 2001), causing global cooling, especially for the ocean surface and high-latitude land areas bordering the North Atlantic and North Pacific Oceans (Bond et al., 1997, 2001; Xu et al., 2014). This triggered IRD discharge events in the North Atlantic and generated global climate variability on centennial to millennial timescales (Bond et al., 1997, 2001; Xu et al., 2014). In East Asia, ocean-atmosphere feedbacks, such as El Niño–Southern Oscillation (ENSO), may have amplified the initial solar forcing to produce persistent sea surface temperature (SST) anomalies in the North Pacific, causing changes in the East Asian monsoon intensity (Ruzmaikin, 1999; Emile-Geay et al., 2007; Xie et al., 2009; T. Zhou et al., 2011; X. Zhou et al., 2011; Xu et al., 2014; Liu et al., 2019). Directly related to variations in monsoonal precipitation, water-table dynamics in the Hongshuipao peatland were influenced by those processes.

In summary, the diatom-based water-table reconstructions from the Hongshuipao peatland show the influence of solar irradiation on climatic and hydrological changes at the EASM margin in northeastern China. Possibly triggered by solar irradiation anomalies and perhaps associated with ocean-atmosphere feedbacks (i.e. ENSO), the peatland hydrological processes at the EASM margin display periodic oscillation at the frequency of ~500-year.

5. Conclusions

Diatom assemblage data from the Hongshuipao peatland document paleohydrological changes at the northern margin of the East Asian summer monsoon. Three main stages that consisted of a higher water-table period (5100–3500 cal. yr BP), a stable water-table stage (2800–-1500 cal. yr BP), and fluctuating conditions since 1500 cal. yr BP are clearly marked in the diatom record.

PCA results suggest that (1) variations in peatland diatom assemblages are primarily associated with water-table changes in the peatland. Comparisons between our data and regional paleoclimate records illustrate that (2) the peatland water-tables changes are in good agreement with the East Asian summer monsoon evolution rather than influenced by peatland site-specific conditions. (3) A statistically significant periodicity of 470-year is detected in the water-table records, which may be linked to solar-forcing parameters. In addition, (4) the major wet (dry) phases of the water-table generally occur at times of higher (lower) sunspot numbers, suggesting a persistent influence of solar forcing on regional hydrological dynamics at the East Asian monsoon margin.

CRediT authorship contribution statement

Nannan Li: Conceptualization, Methodology, Investigation, Formal analysis, Writing - original draft, Writing - review & editing. **Mengzhen Li:** Methodology, Investigation, Writing - original draft. **Dorothy Sack:** Writing - original draft, Writing - review & editing. **Wengang Kang:** Methodology, Investigation, Formal analysis. **Lina Song:** Data curation, Methodology. **Yue Yang:** Data curation, Methodology. **Yazhuo Zong:** Data curation, Methodology. **Dongmei Jie:** Conceptualization, Investigation, Writing - review & editing, Funding acquisition.

Declaration of competing interest

No conflict of interest exists in the submission of this manuscript, and the manuscript is approved by all authors for publication.

Acknowledgments

We thank Xuedong Zhang (Wuchagou Forestry Bureau of Inner Mongolia Autonomous Region) and Hongpeng Zhang (NENU) for their assistance in the field work. We would thank four anonymous reviewers for suggestions and comments that greatly improved the manuscript. This work was financially supported by the National Natural Science Foundation of China (Grant No. 41771214, 41471164, 41971100), the National Key Research and Development Program of China (Grant No. 2016YFA0602301).

Appendix A. Supplementary data

Supplementary data to this article can be found online at https://doi.org/10.1016/j.scitotenv.2020.138272.

References

An, Z., 2000. The history and variability of the East Asian paleomonsoon climate. Quat. Sci. Rev. 19, 171–187.
An, Z., Wu, G., Li, J., Sun, Y., Liu, Y., Zhou, W., Cai, Y., Duan, A., Li, L., Mao, J., Cheng, H., Shi, Z., Tan, L., Yan, H., Ao, H., Chang, H., Feng, J., 2015. Global Monsoon dynamics and climate change. Annu. Rev. Earth Planet. Sci. 43, 29–77.
Berger, A., Loutre, M.F., 1991. Insolation values for the climate of the last 10 million years. Quat. Sci. Rev. 10, 297–317.
Blaauw, M., Christen, J.A., 2005. Radiocarbon peat chronologies and environmental change. Appl. Stat. 54, 805–816.
Blaauw, M., Christen, J.A., 2011. Flexible paleoclimate age-depth models using an autoregressive gamma process. Bayesian Anal. 6, 457–474.
Bond, G.C., Showers, W., Cheseby, M., Lotti, R., Almasi, P., deMenocal, P., Priore, P., Cullen, H., Hajdas, I., Bonani, G., 1997. A pervasive millennial-scale cycle in North Atlantic Holocene and glacial climates. Science 278 (5341), 1257–1266.
Bond, G.C., Kromer, B., Beer, J., Muscheler, R., Evans, M.N., Showers, W., Hoffmann, S., Lotti-Bond, R., Hajdas, I., Bonani, G., 2001. Persistent solar influence on North Atlantic climate during the Holocene. Science 294 (5549), 2130–2136.
Chambers, F.M., Charman, D.J., 2004. Holocene environmental change: contributions from the peatland archive. Holocene 14 (1), 1–6.
Chambers, F.M., Beilman, D.W., Yu, Z., 2011. Methods for determining peat humification and for quantifying peat bulk density, organic matter and carbon content for palaeostudies of climate and peatland carbon dynamics. Mires Peat 7 (Article 7, 10pp).
Chambers, F.M., Booth, R.K., De Vleeschouwer, F., Lamentowicz, M., Le Roux, G., Mauquoy, D., Nichols, J.E., van Geel, B., 2012. Development and refinement of proxy-climate indicators from peats. Quat. Int. 268, 21–33.
Chao, W.C., Chen, B., 2001. The origin of monsoons. J. Atmos. Sci. 58, 3497–3507.
Charman, D.J., 2007. Summer water deficit variability controls on peatland water-table changes: implications for Holocene palaeoclimate reconstructions. Holocene 17, 217–227.
Chen, X., Qin, Y., Stevenson, M.A., McGowan, S., 2014. Diatom communities along pH and hydrological gradients in three montane mires, central China. Ecol. Indic. 45, 123–129.
Chen, X., Bu, Z., Stevenson, M.A., Cao, Y., Zeng, L., Qin, B., 2016. Variations in diatom communities at genus and species levels in peatlands (central China) linked to microhabitats and environmental factors. Sci. Total Environ. 568, 137–146.
Chen, X., McGowan, S., Bu, Z., Yang, X., Cao, Y., Bai, X., Zeng, L., Liang, J., Qiao, Q., 2020. Diatom-based water-table reconstruction in Sphagnum peatlands of northeastern China. Water Res. 174, 115648.
China Meteorological Data Service Center, 2019. Monthly averaged climate data of A'er'shan meteorological station (1981 to 2010). China Meteorological Data Service Centerhttp://data.cma.cn/.
Cosford, J., Qing, H., Mattey, D., Eglinton, B., Zhang, M., 2009. Climatic and local effects on stalagmite $\delta^{13}C$ values at Lianhua Cave, China. Palaeogeogr. Palaeoclimatol. Palaeoecol. 280, 235–244.
Cui, M., Luo, Y., Sun, X., 2006. Paleoenvironmental and paleoclimate changes in Hani Lake, Jilin since 5ka BP. Mar. Geol. Quat. Geol. 26 (5), 117–122 (in Chinese).
Ding, R., Ha, K., Li, J., 2010. Interdecadal shift in the relationship between the East Asian summer monsoon and the tropical Indian Ocean. Clim. Dyn. 34, 1059–1071.
Emile-Geay, J., Cane, M., Seager, R., Kaplan, A., Almasi, P., 2007. El Niño as a mediator of the solar influence on climate. Paleoceanography 22. https://doi.org/10.1029/2006PA001304 PA3210.
Fan, J., Xiao, J., Wen, R., Zhang, S., Wang, X., Cui, L., Li, H., Xue, D., Yamagata, H., 2016. Droughts in the East Asian summer monsoon margin during the last 6 kyrs: link to the North Atlantic cooling events. Quat. Sci. Rev. 151, 88–99.
Fan, J., Xiao, J., Wen, R., Zhang, S., Wang, X., Cui, L., Yamagata, H., 2017. Carbon and nitrogen signatures of sedimentary organic matter from Dali Lake in Inner Mongolia: implications for Holocene hydrological and ecological variations in the East Asian summer monsoon margin. Quat. Int. 452, 65–78.
Finkelstein, S.A., Bunbury, J., Gajewski, K., Wolfe, A.P., Adams, J.K., Devlin, J.E., 2014. Evaluating diatom-derived Holocene pH reconstructions for Arctic lakes using an expanded 171-lake training set. J. Quat. Sci. 29, 249–260.

Fukumoto, Y., Kashima, K., Orkhonselenge, A., Ganzorig, U., 2012. Holocene environmental changes in northern Mongolia inferred from diatom and pollen records of peat sediment. Quat. Int. 254, 83–91.

Gaiser, E.E., Rühland, K.M., 2010. Diatoms as indicators of environmental change in wetlands and peatlands. In: Smol, J.P., Stoermer, E.F. (Eds.), The Diatoms: Applications for the Environmental and Earth Sciences. Cambridge University Press, Cambridge, pp. 473–496.

Gaiser, E.E., Philippi, T.E., Taylor, B.E., 1998. Distribution of diatoms among intermittent ponds on the Atlantic Coastal Plain: development of a model to predict drought periodicity from surface sediment assemblages. J. Paleolimnol. 20, 71–90.

Gao, C., He, J., Zhang, Y., Cong, J., Han, D., Wang, G., 2018. Fire history and climate characteristics during the last millennium of the Great Hinggan Mountains at the monsoon margin in northeastern China. Glob. Planet. Change 162, 313–320.

Grimm, E.C., 1987. CONISS: a Fortran 77 program for stratigraphically constrained cluster analysis by the method of the incremental sum of squares. Comput. Geosci. 13, 13–35.

Grimm, E.C., 1992. TILIA and TILIA*GRAPH Computer Program. Illinois State Museum, Springfield, IL.

Gross, E.M., Bécares, E., 2020. Large-scale geographical and environmental drivers of shallow lake diatom metacommunities across Europe. Sci. Total Environ. 707, 135887.

Grundling, P., Clulow, A.D., Price, J.S., Everson, C.S., 2015. Quantifying the water balance of Mfabeni Mire (iSimangaliso Wetland Park, South Africa) to understand its importance, functioning and vulnerability. Mires Peat 16, 1–18 Article 12.

Guo, L., Xiong, S., Ding, Z., Jin, G., Wu, J., Ye, W., 2018. Role of the mid-Holocene environmental transition in the decline of late Neolithic cultures in the deserts of NE China. Quat. Sci. Rev. 190, 98–113.

Haigh, J.D., 1996. The impact of solar variability on climate. Science 272, 981e984.

Hao, Q., Liu, H., Liu, X., 2016. Pollen-detected altitudinal migration of forests during the Holocene in the mountainous forest–steppe ecotone in northern China. Palaeogeogr. Palaeoclimatol. Palaeoecol. 46, 70–77.

Hargan, K.E., Rühland, K.M., Paterson, A.M., Finkelstein, S.A., Holmquist, J.R., MacDonald, G.M., Keller, W., Smol, J.P., 2015a. The influence of water-table depth and pH on the spatial distribution of diatom species in peatlands of the Boreal Shield and Hudson Plains, Canada. Botany 93, 57–74.

Hargan, K.E., Rühland, K.M., Paterson, A.M., Holmquist, J., MacDonald, G.M., Bunbury, J., Finkelstein, S.A., Smol, J.P., 2015b. Long-term successional changes in peatlands of the Hudson Bay Lowlands, Canada inferred from the ecological dynamics of multiple proxies. Holocene 25 (1), 92–107.

Hong, Y., Jiang, H., Liu, T., Zhou, L., Beer, J., Li, H., Leng, X., Hong, B., Qin, X., 2000. Response of climate to solar forcing recorded in a 6000-year $\delta^{18}O$ time series of Chinese peat cellulose. Holocene 10, 1–7.

Hong, Y., Wang, Z., Jiang, H., Lin, Q., Hong, B., Zhu, Y., Wang, Y., Xu, L., Leng, X., Li, H., 2001. A 6000-year record of changes in drought and precipitation in northeastern China based on a $\delta^{13}C$ time series from peat cellulose. Earth Planet. Sci. Lett. 185, 111–119.

Ingram, H.A.P., 1983. Hydrology. In: Gore, A.J.P. (Ed.), Mires: Swamp, Bog, Fen and Moor, Ecosystems of the World, 4A, General Studies. Elsevier, Amsterdam, pp. 67–158.

Kassambara, A., Mundt, F., 2019. R package "factoextra": extract and visualize the results of multivariate data analyses (version 1.0.6). Available from. http://www.sthda.com/english/rpkgs/factoextra.

Kelly, M.G., 1998. Use of the trophic diatom index to monitor eutrophication in rivers. Water Res. 32, 236–242.

Kokfelt, U., Struyf, E., Randsalu, L., 2009. Diatoms in peat – dominant producers in a changing environment? Soil Biol. Biochem. 41, 1764–1766.

Krammer, K., Lange-Bertalot, H., 1986–1991. Bacillariophyceae. In: Ettl, H., Gerloff, J., Heynig, H., Mollenhauer, D. (Eds.), Süßwasserflora von Mitteleuropa. vol. 2(1–4). Gustav Fischer Verlag, Stuttgart/Jena.

Lamb, H.H., 1965. The early medieval warm epoch and its sequel. Palaeogeogr. Palaeoclimatol. Palaeoecol. 1 (65), 13e37.

Lange-Bertalot, H., Bak, M., Witkowski, A., 2011. Diatoms of Europe: Diatoms of the European Inland Waters and Comparable Habitats (Vol. 6. Eunotia and Some Related Genera). A.R.G. Gantner Verlag K.G, Ruggel.

Li, N., Chambers, F.M., Yang, J., Jie, D., Liu, L., Liu, H., Gao, G., Gao, Z., Li, D., Shi, J., Feng, Y., Qiao, Z., 2017. Records of East Asian monsoon activities in northeastern China since 15.6 ka, based on grain size analysis of peaty sediments in the Changbai Mountains. Quat. Int. 447, 158–169.

Lioubimtseva, E., Henebry, G.M., 2009. Climate and environmental change in arid Central Asia: impacts, vulnerability, and adaptations. J. Arid Environ. 73, 963–977.

Liu, H., Xu, L., Cui, H., 2002. Holocene history of desertification along the woodland-steppe border in northern China. Quat. Res. 57, 259–270.

Liu, Q., Li, Q., Wang, L., Chu, G., 2010. Stable carbon isotope record of bulk organic matter from a sediment core at Moon Lake in the middle part of the Daxing'an Mountain range, northeast China during the last 21 ka. Quat. Sci. 30 (6), 1069–1077 (in Chinese).

Liu, H., Lin, Z., Qi, X., Li, Y., Yu, M., Yang, H., Shen, J., 2012. Possible link between Holocene East Asian monsoon and solar activity obtained from the EMD method. Nonlinear Process. Geophys. 19, 421–430.

Liu, H., Yin, Y., Hao, Q., Liu, G., 2014. Sensitivity of temperate vegetation to Holocene development of East Asian monsoon. Quat. Sci. Rev. 98, 126–134.

Liu, H., Gu, Y., Huang, X., Yu, Z., Xie, S., Cheng, S., 2019. A 13,000-year peatland palaeohydrological response to the ENSO-related Asian monsoon precipitation changes in the middle Yangtze Valley. Quat. Sci. Rev. 212, 80–91.

Ma, L., Gao, C., Kattel, G.R., Yu, X., Wang, G., 2018. Evidence of Holocene water level changes inferred from diatoms and the evolution of the Honghe Peatland on the Sanjiang Plain of Northeast China. Quat. Int. 476, 82–94.

Marsh, N., Svensmark, H., 2003. Solar influence on Earth's climate. Space Sci. Rev. 107, 317–325.

Nohe, A., Goffin, A., Tyberghein, L., Lagring, R., De Cauwer, K., Vyverman, W., Sabbe, K., 2020. Marked changes in diatom and dinoflagellate biomass, composition and seasonality in the Belgian Part of the North Sea between the 1970s and 2000s. Sci. Total Environ. 716, 136316.

Piotrowska, N., Blaauw, M., Mauquoy, D., Chambers, F.M., 2011. Constructing deposition chronologies for peat deposits using radiocarbon dating. Mires Peat 7, 1–14 Article 10.

R Core Team, 2017. R: A Language and Environment for Statistical Computing. R Foundation for Statistical Computing, Vienna, Austria URL. https://www.R-project.org.

Reimer, P.J., Bard, E., Bayliss, A., Beck, J.W., Blackwell, P.G., Bronk Ramsey, C., Buck, C.E., Edwards, R.L., Friedrich, M., Grootes, P.M., Guilderson, T.P., Haflidason, H., Hajdas, I., Hatté, C., Heaton, T.J., Hoffmann, D.L., Hogg, A.G., Hughen, K.A., Kaiser, K.F., Kromer, B., Manning, S.W., Niu, M., Reimer, R.W., Richards, D.A., Scott, M.E., Southon, J.R., Turney, C.S.M., van der Plicht, J., 2013. IntCal13 and Marine13 radiocarbon age calibration curves 0–50,000 yr cal BP. Radiocarbon 55 (4), 1869–1887.

Ren, G., 1998. Pollen evidence for increased summer rainfall in the Medieval warm period at Maili, Northeast China. Geophys. Res. Lett. 25, 1931–1934.

Rodríguez-Alcalá, O., Blanco, S., García-Girón, J., Jeppesen, E., Irvine, K., Nõges, P., Nõges, T., Rivera-Rondón, C.A., Catalan, J., 2020. Diatoms as indicators of the multivariate environment of mountain lakes. Sci. Total Environ. 703, 135517.

Rott, E., Duthie, H.C., Pipp, E., 1998. Monitoring organic pollution and eutrophication in the Grand River, Ontario, by means of diatoms. Can. J. Fish. Aquat. Sci. 55, 1443–1453.

RStudio Team, 2016. RStudio: Integrated Development Environment for R. RStudio, Inc, Boston, MA URL:. http://www.rstudio.com.

Rühland, K.M., Smol, J.P., Jasinski, J.P.P., Warner, B.G., 2000. Response of diatoms and other siliceous indicators to the developmental history of a peatland in the Tiksi Forest, Siberia, Russia. Arct. Antarct. Alp. Res. 32, 167–178.

Ruzmaikin, A., 1999. Can El Niño amplify the solar forcing of climate? Geophys. Res. Lett. 26, 2255–2258.

Schulz, M., Mudelsee, M., 2002. REDFIT: estimating red-noise spectra directly from unevenly spaced paleoclimatic time series. Comput. Geosci. 28, 421–426.

Scuderi, L.A., Yang, X., Ascoli, S.E., Li, H., 2019. The 4.2 ka BP Event in northeastern China: a geospatial perspective. Clim. Past 15, 367–375.

Serieyssol, K., Chatelard, S., Cubizolle, H., 2010–2011. Diatom fossils in mires: a protocol for extraction, preparation and analysis in palaeoenvironmental studies. Mires Peat 7, 1–11.

Shindell, D., Rind, D., Balachandran, N., Lean, J., Lonergan, P., 1999. Solar cycle variability, ozone, and climate. Science 284, 305e308.

Shindell, D.T., Schmidt, G.A., Mann, M.E., Rind, D., Waple, A., 2001. Solar forcing of regional climate change during the Maunder Minimum. Science 294, 2149–2152.

Sivakumar, M.V.K., 2007. Interactions between climate and desertification. Agric. For. Meteorol. 142, 143–155.

Solanki, S.K., Usoskin, I.G., Kromer, B., Schüssler, M., Beer, J., 2004. Unusual activity of the Sun during recent decades compared to the previous 11,000 years. Nature 431, 1084–1087.

Stebich, M., Rehfeld, K., Schlütz, F., Tarasov, P.E., Liu, J., Mingram, J., 2015. Holocene vegetation and climate dynamics of NE China based on the pollen record from Sihailongwan Maar Lake. Quat. Sci. Rev. 124, 275–289.

Steinhilber, F., Abreu, J.A., Beer, J., Brunner, I., Christl, M., Fischer, H., Heikkilä, U., Kubik, P.W., Mann, M., McCracken, K.G., Miller, H., Miyahara, H., Oerter, H., Wilhelms, F., 2012. 9,400 years of cosmic radiation and solar activity from ice cores and tree rings. Proc. Natl. Acad. Sci. U. S. A. 109, 5967–5971.

Stuiver, M., Braziunas, T.F., 1993. Modeling atmospheric ^{14}C influence and ^{14}C ages of marine samples to 10,000 BC. Radiocarbon 35, 137–189.

Stuiver, M., Reimer, P.J., 1993. Extended ^{14}C database and revised CALIB radiocarbon calibration program. Radiocarbon 35, 215–230.

Stuiver, M., Grootes, P., Braziunas, T., 1995. The GISP2 $\delta^{18}O$ climate record of the past 16,500 years and the role of the sun, ocean, and volcanoes. Quat. Res. 44, 341–354.

Swindles, G.T., Plunkett, G., Roe, H.M., 2007. A multiproxy climate record from a raised bog in County Fermanagh, Northern Ireland: a critical examination of the link between bog surface wetness and solar variability. J. Quat. Sci. 22, 667–679.

van Dam, H., Mertens, A., Sinkeldam, J., 1994. A coded checklist and ecological indicator values of freshwater diatoms from the Netherlands. Neth. J. Aquat. Ecol. 28, 117–133.

Wang, P., Clemens, S., Beaufort, L., Braconnot, P., Ganssen, G., Jian, Z., Kershaw, P., Sarnthein, M., 2005a. Evolution and variability of the Asian monsoon system: state of the art and outstanding issues. Quat. Sci. Rev. 24, 595–629.

Wang, Y., Cheng, H., Edwards, R.L., He, Y., Kong, X., An, Z., Wu, J., Kelly, M.J., Dykoski, C.A., Li, X., 2005b. The Holocene Asian monsoon: links to solar changes and North Atlantic climate. Science 308, 854–857.

Wang, S., Wen, X., Luo, Y., Dong, W., Zhao, Z., Yang, B., 2007. Reconstruction of temperature series of China for the last 1000 years. Chin. Sci. Bull. 52, 3272–3280.

Wang, P., Wang, B., Cheng, H., Fasullo, J., Guo, Z., Kiefer, T., Liu, Z., 2017. The global monsoon across time scales: mechanisms and outstanding issues. Earth Sci. Rev. 174, 84–121.

Wang, Q., Anderson, N.J., Yang, X., Xu, M., 2020. Interactions between climate change and early agriculture in SW China and their effect on lake ecosystem functioning at centennial timescales over the last 2000 years. Quat. Sci. Rev. 233, 106238.

Wei, T., Simko, V., 2017. R package "corrplot": visualization of a correlation matrix (version 0.84). Available from. https://github.com/taiyun/corrplot.

Wen, R., Xiao, J., Chang, Z., Zhai, D., Xu, Q., Li, Y., Itoh, S., Lomtatidze, Z., 2010. Holocene climate changes in the mid-high-latitude-monsoon margin reflected by the pollen record from Hulun Lake, northeastern Inner Mongolia. Quat. Res. 73, 293–303.

Wen, R., Xiao, J., Fan, J., Zhang, S., Yamagata, H., 2017. Pollen evidence for a mid-Holocene East Asian summer monsoon maximum in northern China. Quat. Sci. Rev. 176, 29–35.

Wu, J., Wang, Y., Dong, J., 2011. Changes in East Asian summer monsoon during the Holocene recorded by stalagmite d18O records from Liaoning Province. Quat. Sci. 31 (6), 990–998 (in Chinese).

Wu, J., Liu, Q., Cui, Q., Xu, D., Wang, L., Shen, C., Chu, G., Liu, J., 2019. Shrinkage of East Asia winter monsoon associated with increased ENSO events since the mid-Holocene. J. Geophys. Res. Atmos. 124, 3839–3848.

Xiao, J., Xu, Q., Nakamura, T., Yang, X., Liang, W., Inouchi, Y., 2004. Holocene vegetation variation in the Daihai Lake region of north-central China: a direct indication of the Asian monsoon climatic history. Quat. Sci. Rev. 23, 1669–1679.

Xiao, J., Si, B., Zhai, D., Itoh, S., Lomtatidze, Z., 2008. Hydrology of Dali Lake in central-eastern Inner Mongolia and Holocene East Asian monsoon variability. J. Paleolimnol. 40, 519–528.

Xiao, J., Zhang, S., Fan, J., Wen, R., Zhai, D., Tian, Z., Jiang, D., 2018. The 4.2 ka BP event: multi-proxy records from a closed lake in the northern margin of the East Asian summer monsoon. Clim. Past 14, 1417–1425.

Xie, S.-P., Hu, K., Hafner, J., Tokinaga, H., Du, Y., Huang, G., Sampe, T., 2009. Indian Ocean capacitor effect on Indo–western Pacific climate during the summer following El Niño. J. Clim. 22, 730–747.

Xu, X., Trumbore, S.E., Zheng, S., Southon, J.R., McDuffee, K.E., Luttgen, M., Liu, J.C., 2007. Modifying a sealed tube zinc reduction method for preparation of AMS graphite targets: reducing background and attaining high precision. Nucl. Instrum. Methods Phys. Res. B 259, 320–329.

Xu, D., Lu, H., Chu, G., Wu, N., Shen, C., Wang, C., Mao, L., 2014. 500-year climate cycles stacking of recent centennial warming documented in an East Asian pollen record. Sci. Rep. 4 (3611), 1–7. https://doi.org/10.1038/srep03611.

Yang, B., Braeuning, A., Johnson, K.R., Shi, Y., 2002. General characteristics of temperature variation in China during the last two millennia. Geophys. Res. Lett. 29. https://doi.org/10.1029/2001gl014485.

Zhang, X., Gong, S., Zhao, T., Arimoto, R., Wang, Y., Zhou, Z., 2003. Sources of Asian dust and role of climate change versus desertification in Asian dust emission. Geophys. Res. Lett. 30, 2272.

Zhang, M., Bu, Z., Jiang, M., Wang, S., Liu, S., Chen, X., Hao, J., Liao, W., 2019. The development of Hani peatland in the Changbai mountains (NE China) and its response to the variations of the East Asian summer monsoon. Sci. Total Environ. 692, 818–832.

Zhou, W., Zheng, Y., Meyers, P.A., Jull, A.J.T., Xie, S., 2010. Postglacial climate-change record in biomarker lipid compositions of the Hani peat sequence, Northeastern China. Earth Planet. Sci. Lett. 294, 37–46.

Zhou, T., Li, B., Man, W., Zhang, L., Zhang, J., 2011a. A comparison of the Medieval Warm Period, Little Ice Age and 20th century warming simulated by the FGOALS climate system model. Chin. Sci. Bull. 56, 3028–3041.

Zhou, X., Zhao, P., Liu, G., Zhou, T., 2011b. Characteristics of decadal-centennial-scale changes in East Asian summer monsoon circulation and precipitation during the Medieval Warm Period and Little Ice Age and in the present day. Chin. Sci. Bull. 56, 3003–3011.

Zhu, K., 1973. Preliminary study on climate change over last 5000 years in China. Sci. China 2 (168e189, in Chinese).

Zhu, S., Ding, P., Wang, N., Shen, C., Jia, G., Zhang, G., 2015. The compact AMS facility at Guangzhou Institute of Geochemistry, Chinese Academy of Sciences. Nucl. Instrum. Methods Phys. Res. B 361, 72–75.